

# Low energy scattering and photoproduction of $\eta$ -mesons on deuterons.

N. V. Shevchenko, V. B. Belyaev

*Joint Institute for Nuclear Research, Dubna, 141980, Russia*

S. A. Rakityansky, S. A. Sofianos

*Physics Dept., University of South Africa, P.O. Box 392*

*Pretoria 0003, South Africa*

and W. Sandhas

*Physikalisches Institut, Universität Bonn, D-53115 Bonn, Germany*

## 1 Introduction

The production of  $\eta$  mesons and their collisions with nuclei have been studied experimentally and theoretically with increasing interest during the last years. To a large extent this is motivated by the fundamental problem of charge-symmetry breaking of strong interaction [1]. Another relevant questions concerns the nature of  $S_{11}(1535)$ -resonance [2] and the possible formation of  $\eta$ -nucleus quasi-bound states [3]. It is worth mentioning that according to [4] the mean free path of  $\eta$  mesons in a nuclear medium is about 2 fm, *i.e.*, less than the size of a typical nucleus. A necessary condition for the existence of  $\eta$ -nuclei, hence, appears to be satisfied.

For the calculation of these states various model treatments were employed, among them the optical potential method [5, 6], the Green's function method [7], the modified multiple scattering theory [8] and few-body calculations [9] – [11]. The predictions concerning the possibility of  $\eta$ -mesic nucleus formation are very diverse. One obvious reason for such a diversity is the poor knowledge of the  $\eta N$  forces. Another reason comes from the differences among the employed approximations some of which might be faulty in view of the resonant character of the  $\eta N$  dynamics and the delicacy of the quasi-bound state problem.

In the present paper we treat the  $\eta$ -deuteron system on the basis of the exact few-body Alt-Grassberger-Sandhas (AGS) equations. The Faddeev-type coupling of these equations guarantees uniqueness of their solutions. Moreover, as equations for the elastic and rearrangement operators they are well-defined in momentum space, providing thus the desired scattering amplitudes in a most direct and technically reliable manner. The advantage of working with coupled equations involving the elastic and rearrangement

operators of the final state, is not only suggested by questions of uniqueness, but also by the relevance of rescattering effects which were found to give a significant contribution to the corresponding amplitude [12].

## 2 AGS formalism

In terms of the AGS transition operator  $U_{11}$  the  $\eta d$  elastic scattering amplitude is represented as

$$f(\mathbf{p}'_1, \mathbf{p}_1; z) = -(2\pi)^2 M_1 \langle \mathbf{p}'_1; \psi_d | U_{11}(z) | \mathbf{p}_1; \psi_d \rangle \quad (1)$$

with the on-energy-shell conditions  $|\mathbf{p}'_1| = |\mathbf{p}_1|$  and  $z = p_1^2/2M_1 + E_d$  with  $E_d$  being the deuteron energy. Here the subscript 1 labels the  $\eta(NN)$  partition and the  $\eta$ -deuteron channel. The transition operator  $U_{11}$  obeys the system of AGS equations

$$U_{\beta\alpha}(z) = (1 - \delta_{\beta\alpha})G_0^{-1}(z) + \sum_{\gamma=1}^3 (1 - \delta_{\beta\gamma})T_\gamma(z)G_0(z)U_{\gamma\alpha}(z), \quad (2)$$

with  $G_0(z)$  being the free resolvent (Green's operator) of the three particles involved. This set of equations couples all  $3 \times 3$  elastic and rearrangement operators  $U_{\alpha\alpha}$  and  $U_{\beta\alpha}$ . Here each of the subscripts runs through the values 1, 2 and 3, indicating the two-fragment partitions (1,23), (2,31) and (3,12) respectively. Therefore,  $U_{11}$  describes the elastic transition  $1(23) \rightarrow 1(23)$ , while  $U_{21}$  represents the rearrangement process  $1(23) \rightarrow 2(13)$ . These subscripts are also used in the complementary notation to label the two-body T-operator  $t_\alpha(z)$  of the  $(\beta\gamma)$  pair, for instance  $t_1(z) = t_{NN}(z)$ . It should be noticed, however, that it is not this genuine two-body operator which enters the AGS equations, but the operator

$$T_\alpha(z) = t_\alpha(z - \mathbf{q}_\alpha^2/2M_\alpha), \quad (3)$$

which is to be understood as the two-body operator embedded in the three-body space, with the relative kinetic energy operator  $\mathbf{q}_\alpha^2/2M_\alpha$  of particle  $\alpha$  being subtracted from the total energy variable  $z$ . Considered in momentum space, (3) thus reads

$$\langle \mathbf{p}'_\alpha, \mathbf{q}'_\alpha | T_\alpha(z) | \mathbf{p}_\alpha, \mathbf{q}_\alpha \rangle = \delta(\mathbf{q}'_\alpha - \mathbf{q}_\alpha) \langle \mathbf{p}'_\alpha | t_\alpha(z - \mathbf{q}_\alpha^2/2M_\alpha) | \mathbf{p}_\alpha \rangle, \quad (4)$$

where  $\mathbf{p}_\alpha$  and  $\mathbf{q}_\alpha$  are the Jacobi momenta of the pair  $\alpha$  and the spectator  $\alpha$  respectively, and  $M_\alpha$  is the corresponding reduced mass.

For both  $T_{\eta N}$  and  $T_{NN}$  we used one-term separable forms

$$T_\alpha(z) = |\chi_\alpha\rangle \tau_\alpha(z) \langle \chi_\alpha|. \quad (5)$$

For the  $NN$  subsystem Eq. (5) implies that the asymptotic wave function is related to the form-factor  $|\chi_1\rangle$  according to

$$|\mathbf{p}_1; \psi_d\rangle = G_0(z) |\chi_1\rangle | \mathbf{p}_1 \rangle. \quad (6)$$

Due to (5) and (6) the scattering amplitude (1) can be rewritten as

$$f(\mathbf{p}'_1, \mathbf{p}_1; z) = -(2\pi)^2 M_1 \langle \mathbf{p}'_1 | X_{11}(z) | \mathbf{p}_1 \rangle, \quad (7)$$

where the operators  $X_{\beta\alpha}$ , defined as

$$X_{\beta\alpha}(z) = \langle \chi_\beta | G_0(z) U_{\beta\alpha}(z) G_0(z) | \chi_\alpha \rangle ,$$

obey the system of equations

$$X_{\beta\alpha}(z) = Z_{\beta\alpha}(z) + \sum_{\gamma=1}^3 Z_{\beta\gamma}(z) \tau_\gamma \left( z - \frac{p_\gamma^2}{2M_\gamma} \right) X_{\gamma\alpha}(z) \quad (8)$$

with

$$Z_{\beta\alpha}(z) = (1 - \delta_{\beta\alpha}) \langle \chi_\beta | G_0(z) | \chi_\alpha \rangle .$$

The identity of the nucleons implies that  $X_{31} = X_{21}$ ,  $\tau_3 = \tau_2$ , and  $Z_{31} = Z_{21}$ , which reduces the system (8) to two coupled equations

$$X_{11}(z) = 2Z_{12}(z)\tau_2 \left( z - \frac{p_2^2}{2M_2} \right) X_{21}(z) , \quad (9)$$

$$X_{21}(z) = Z_{21}(z) + Z_{21}(z)\tau_1 \left( z - \frac{p_1^2}{2M_1} \right) X_{11}(z) + Z_{23}(z)\tau_2 \left( z - \frac{p_2^2}{2M_2} \right) X_{21}(z) .$$

Eventually, after making the  $S$ -wave projection of the matrix elements  $\langle \mathbf{p}'_\beta | X_{\beta\alpha} | \mathbf{p}_\alpha \rangle$  and  $\langle \mathbf{p}'_\beta | Z_{\beta\alpha} | \mathbf{p}_\alpha \rangle$ , we end up with one-dimensional integral equations which can be solved numerically.

### 3 Two-body T-matrices

The  $S$ -wave nucleon-nucleon separable potential is adopted from Ref.[13] with its parameters slightly modified to be consistent with more recent  $NN$  data (see Ref.[11]). The  $\eta$ -nucleon  $T$ -matrix is taken in the form

$$t_{\eta N}(p', p; z) = (p'^2 + \alpha^2)^{-1} \frac{\lambda}{(z - E_0 + i\Gamma/2)} (p^2 + \alpha^2)^{-1} \quad (10)$$

consisting of two vertex functions and the  $S_{11}$ -propagator in between [10]. It corresponds to the process  $\eta N \rightarrow S_{11} \rightarrow \eta N$  which at low energies is dominant. The range parameter  $\alpha = 3.316 \text{ fm}^{-1}$  was determined in Ref. [14], while  $E_0$  and  $\Gamma$  are the parameters of the  $S_{11}$  resonance [15],

$$E_0 = 1535 \text{ MeV} - (m_N + m_\eta) , \quad \Gamma = 150 \text{ MeV} .$$

The strength parameter  $\lambda$  is chosen to reproduce the  $\eta$ -nucleon scattering length  $a_{\eta N}$ ,

$$\lambda = \frac{\alpha^4 (E_0 - i\Gamma/2)}{(2\pi)^2 \mu_{\eta N}} a_{\eta N} . \quad (11)$$

the imaginary part of which accounts for the flux losses into the  $\pi N$  channel.

The two-body scattering length  $a_{\eta N}$  is not accurately known. Different analyses [16] provided for  $a_{\eta N}$  the values in the range

$$0.27 \text{ fm} \leq \text{Re } a_{\eta N} \leq 0.98 \text{ fm} , \quad 0.19 \text{ fm} \leq \text{Im } a_{\eta N} \leq 0.37 \text{ fm} . \quad (12)$$

Recently, however, most of the authors agreed that  $\text{Im } a_{\eta N}$  is around 0.3 fm. But for  $\text{Re } a_{\eta N}$  the estimates are still very different (compare, for example, Refs. [17] and [18]). Most of the results presented in this paper are, therefore, obtained using  $\text{Im } a_{\eta N} = 0.3 \text{ fm}$  and several values of  $\text{Re } a_{\eta N}$  within the above interval.

We solved Eqs. (9) for  $\eta d$  collision energies varying from zero ( $\eta d$ -threshold,  $z = E_d$ ) up to 22 MeV by replacing the integrals by Gaussian sums. As is well known (see, for example, [19]), the kernels of these equations, when expressed in momentum representation, have moving logarithmic singularities for  $z > 0$ . In the numerical procedure, we handle it with the method suggested in Ref.[20]. The main idea of this method consists in interpolating the unknown solutions (in the area covering the singular points) by certain polynomials and subsequent analytic integration of the singular part of the kernels.

## 4 Scattering results

The results of our calculations are presented in Figs. 1–4 and in Table 1. In Fig. 1 the energy dependence of the  $\eta d$  phase-shifts for five different choices of  $\text{Re } a_{\eta N}$  is shown. The curves correspond (starting from the lowest one) to  $\text{Re } a_{\eta N} = 0.55 \text{ fm}$ , 0.65 fm, 0.725 fm, 0.75 fm, and 0.85 fm. The larger this value, the stronger is the  $\eta N$  attraction. The

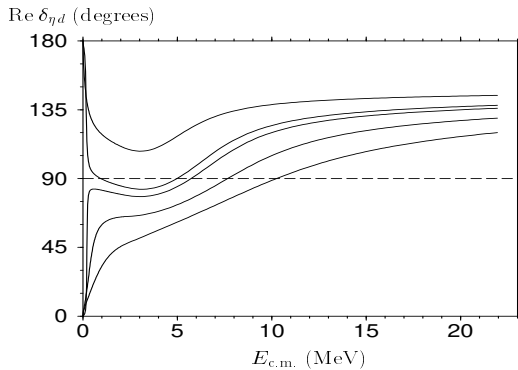


Figure 1: Real part of the  $\eta$ -deuteron phase-shift as a function of the collision energy.

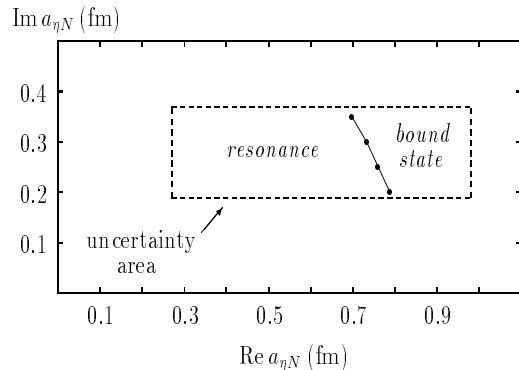


Figure 2: The critical values of  $a_{\eta N}$  (filled circles) to the right of which the  $\eta d$ -system can be bound.

change in the character of these curves, hence, reflects the growth of the attractive force between the  $\eta$  meson and the nucleon. The lower three curves for  $\text{Re } \delta_{\eta d}$  corresponding to the smaller values of  $\text{Re } a_{\eta N}$  start from zero, the two curves corresponding to the strong attraction start from  $\pi$ . According to Levinson's theorem, the phase shift at threshold energy is equal to the number of bound states  $n$  times  $\pi$ . We found that the transition from the lower family of the curves to the upper one happens at the critical value  $\text{Re } a_{\eta N}$

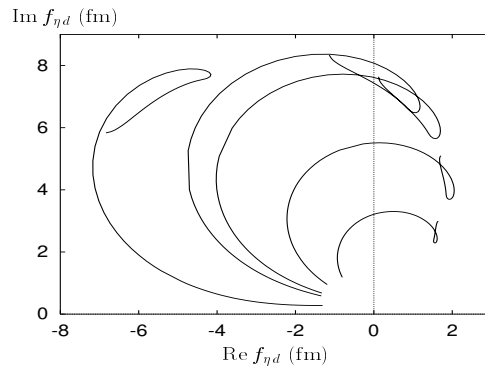
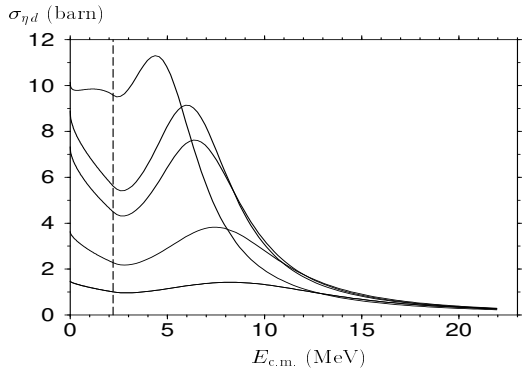


Figure 3: Total cross-section for elastic  $\eta d$

Figure 4: Argand plot for the  $\eta d$  elastic scattering amplitude.

$a_{\eta N} = 0.733$  fm. Therefore, the  $\eta N$  force, which generates  $\text{Im } a_{\eta N} = 0.3$  fm and  $\text{Re } a_{\eta N} > 0.733$  fm, is sufficiently attractive to bind  $\eta$  inside the deuteron.

For three other choices of  $\text{Im } a_{\eta N}$  within the uncertainty interval, namely, 0.20 fm, 0.25 fm, and 0.35 fm, the corresponding critical values of  $\text{Re } a_{\eta N}$  turned out to be 0.788 fm, 0.761 fm, and 0.698 fm. In the complex  $a_{\eta N}$ -plane (see Fig. 2) the corresponding points form a curve separating the uncertainty area (given by formulae (12), dashed rectangle) into two parts. If  $a_{\eta N}$  is to the right of this curve, the strength of  $\eta N$  attraction is sufficient for  $\eta d$  bound state formation.

$\text{Re } a_{\eta N}$ (fm)	$E_{\eta d}^{\text{res}}$ (MeV)	$\Gamma_{\eta d}$ (MeV)
0.55	8.24	9.15
0.65	7.46	8.45
0.675	7.14	7.61
0.70	6.79	6.90
0.725	6.41	6.31
0.75	6.01	5.87
0.85	4.39	5.79
0.90	3.73	6.81

Table 1: Energy and width of the  $\eta d$  resonance for various choices of  $\text{Re } a_{\eta N}$ .

In Fig. 3 we present the result of our calculations of the total cross-section (integrated over the angles) for elastic  $\eta$ -deuteron scattering as a function of collision energy. The five curves correspond (starting from the lowest one) to  $\text{Re } a_{\eta N} = 0.55$  fm, 0.65 fm, 0.725 fm, 0.75 fm, and 0.85 fm. The dashed line indicates the deuteron break-up threshold. The peaks in the energy dependence of the total elastic cross-section indicate that a resonance appears in the  $\eta d$ -system. Of course, not every maximum of the cross-section is a resonance, but we plotted the Argand plots also (Fig. 4) for the  $\eta d$  elastic scattering amplitude in the energy interval from 0 to 22 MeV. The five curves correspond (from right to left) to  $\text{Re } a_{\eta N} = 0.55$  fm, 0.65 fm, 0.725 fm, 0.75 fm, and 0.85 fm. When the energy increases the corresponding points move anticlockwise. So that the Argand plots prove

that the maxima we found are resonances. Their positions and widths for various choices of  $\text{Re } a_{\eta N}$  are given in Table 1. It should be noted that, while the resonance energy is determined in our calculations exactly (as the maximum of the function  $\sin^2 \text{Re } \delta_{\eta d}$ ), the corresponding width is obtained by fitting the cross-section with a Breit-Wigner curve. Therefore, the values of  $\Gamma_{\eta d}$  given in Table 1 should be considered only as rough estimates.

The resonant behavior of  $\eta d$  elastic scattering should be seen in various processes involving  $\eta d$ -system in their final states, such as  $\gamma d \rightarrow \eta d$  and  $np \rightarrow \eta d$ . Indeed, the corresponding amplitudes  $\langle \psi_{\text{out}} | \mathcal{O} | \psi_{\text{in}} \rangle$  involve the  $\eta d$  wave function  $\psi_{\text{out}}$  which, in the vicinity of the resonance, strongly depends on the total energy. Its resonant growth at short distances may enhance the transition probability. To check this suggestion we performed the calculations of the  $\gamma d \rightarrow \eta d$  reaction.

## 5 Photoproduction of $\eta$ -mesons

Theoretical analysis of  $(\gamma, \eta)$ -reactions on nuclei is hampered by the three major problems: the unknown off-shell behavior of the two-body  $\gamma N \rightarrow \eta N$  amplitude, inaccuracies in the description of the nuclear target as a many-body system, and rescattering effects in the final state. The simplest is, of course, the process of coherent  $\eta$  photoproduction on deuteron. There are many theoretical studies devoted to  $(\gamma, \eta)$  reactions on deuteron. Early attempts to go beyond a simple impulse approximation led to very different conclusions [21] – [23] as do more recent approaches based on the effective two-body formulations [24], [25]. Moreover, the experimental cross-section [26] of the reaction

$$\gamma + d \rightarrow \eta + d \quad (13)$$

in the near-threshold region is far above these theoretical predictions. Therefore, a reliable description of  $\eta$  photoproduction on deuteron on the basis of exact equations is desirable.

## 6 Formalism

To consider reaction (13), we employ the exact Alt-Grassberger-Sandhas formalism modified to include the electromagnetic interaction. A photon can be introduced into this formalism by considering the  $\eta N$  and  $\gamma N$  states as two different channels of the same system. This means that we should replace the T-operator  $t_{\eta N}$  by the  $2 \times 2$  matrix. It is clear, that such replacements of the kernels of integral equations (2) lead to the corresponding solutions having a similar matrix form

$$t_{\eta N} \rightarrow \begin{pmatrix} t^{\gamma\gamma} & t^{\gamma\eta} \\ t^{\eta\gamma} & t^{\eta\eta} \end{pmatrix} \quad U_{\alpha\beta} \rightarrow \begin{pmatrix} W_{\alpha\beta}^{\gamma\gamma} & W_{\alpha\beta}^{\gamma\eta} \\ W_{\alpha\beta}^{\eta\gamma} & W_{\alpha\beta}^{\eta\eta} \end{pmatrix}. \quad (14)$$

Here  $t^{\gamma\gamma}$  describes the Compton scattering,  $t^{\eta\gamma}$  the photoproduction process, and  $t^{\eta\eta}$  the elastic  $\eta N$  scattering<sup>1</sup>.

---

<sup>1</sup>Another method of treatment electromagnetic process of the type (13) in the frame of AGS equations was used in Ref.[27].

It is technically more convenient to consider the reaction of  $\eta$ -photoabsorption, which is inverse to reaction (13). Then the photoproduction cross-section can be obtained by applying the detailed balance principle. We are interested in the coherent process, therefore we need the amplitude  $W_{11}^{\gamma\eta}$  obeying the equation

$$\begin{pmatrix} W_{11}^{\gamma\gamma} & W_{11}^{\gamma\eta} \\ W_{11}^{\eta\gamma} & W_{11}^{\eta\eta} \end{pmatrix} = \begin{pmatrix} T_2^{\gamma\gamma} & T_2^{\gamma\eta} \\ T_2^{\eta\gamma} & T_2^{\eta\eta} \end{pmatrix} G_0 \begin{pmatrix} W_{21}^{\gamma\gamma} & W_{21}^{\gamma\eta} \\ W_{21}^{\eta\gamma} & W_{21}^{\eta\eta} \end{pmatrix} + \begin{pmatrix} T_3^{\gamma\gamma} & T_3^{\gamma\eta} \\ T_3^{\eta\gamma} & T_3^{\eta\eta} \end{pmatrix} G_0 \begin{pmatrix} W_{31}^{\gamma\gamma} & W_{31}^{\gamma\eta} \\ W_{31}^{\eta\gamma} & W_{31}^{\eta\eta} \end{pmatrix}. \quad (15)$$

In the first order on electromagnetic interaction:

$$W_{11}^{\gamma\eta} \approx T_2^{\gamma\eta} G_0(z) W_{21}^{\eta\eta} + T_3^{\gamma\eta} G_0(z) W_{31}^{\eta\eta} \quad (16)$$

and we can see, that in above approximation the transition operator  $W_{11}^{\gamma\eta}$  can be found not from an equation, but from the expression (16). It is physically clear since in the first order on electromagnetic interaction the only contributions are from the  $\eta$ -meson rescattering which is described by the  $W_{21}^{\eta\eta}$  and  $W_{31}^{\eta\eta}$  operators.

It was experimentally proven [28] that at low energies the reaction  $\gamma N \rightarrow \eta N$  mainly goes via formation of the  $S_{11}$ -resonance, which means that  $t^{\gamma\eta}$  in the near-threshold region can be written in a separable form similar to (5). To construct such separable T-matrix, we used the results of Ref. [29] where  $t^{\gamma\eta}$  was obtained as an element of a multi-channel T-matrix which simultaneously describes data for the processes

$$\begin{aligned} \pi + N &\rightarrow \pi + N, & \pi + N &\rightarrow \eta + N, \\ \gamma + N &\rightarrow \pi + N, & \gamma + N &\rightarrow \eta + N \end{aligned}$$

on the energy shell in the  $S_{11}$ -channel. For our calculations, we extended this T-matrix off the energy shell,

$$t_{off}^{\gamma\eta}(p', p; E) = \frac{\kappa^2 + E^2}{\kappa^2 + p'^2} t_{on}^{\gamma\eta}(E) \frac{\alpha^2 + 2\mu E}{\alpha^2 + p^2}, \quad (17)$$

using the Yamaguchi form-factors which become unit on the energy shell. Here  $\kappa$  stands for some unknown parameter. It is known, that  $t^{\gamma\eta}$  is different for neutron and proton, we assumed that they have the same functional form and differ by a constant factor  $t_n^{\gamma\eta} = A t_p^{\gamma\eta}$ . A multipole analysis [30] gives for this factor the following estimate:  $A = -0.84 \pm 0.15$ .

## 7 Photoproduction results

As was expected, our calculations revealed very strong final state interaction in the reaction (13). A comparison of the corresponding cross-sections obtained by solving the AGS equations and by using the Impulse Approximation (IA) is given in Fig. 5, where the IA-results are multiplied by 10. Besides the fact that the IA-curve is generally an order of magnitude lower, it does not show a resonant enhancement which is clearly seen when all

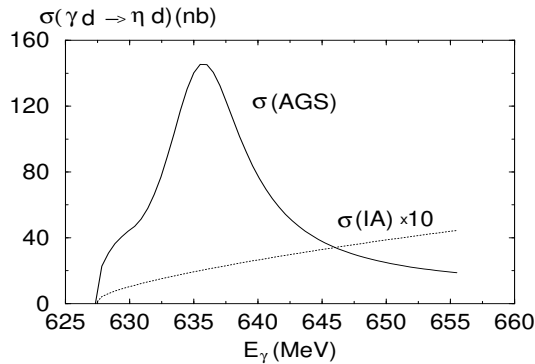


Figure 5: Total cross-section, calculated within a rigorous few-body theory (AGS) and Impulse Approximation (IA).

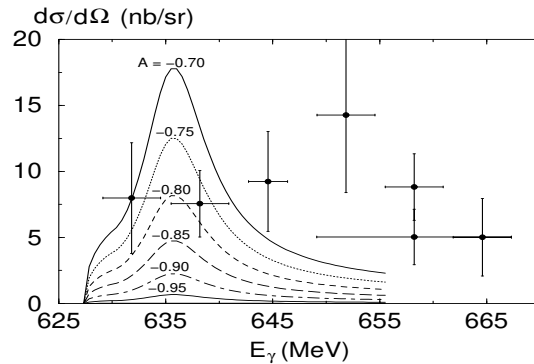


Figure 6: Differential cross-section ( $\Theta_\eta^{cm} = 90^\circ$ ), calculated with different choices of the ratio  $A$ .

the rescattering and re-arrangement processes are taken into account. In this connection, it should be noted that experimental data [26] for the reaction (13), given in Figs. 6 – 8 show a pronounced enhancement of the differential cross-section at low energies.

In order to examine a dependence of our calculations on the choice of the parameters of the T-matrices  $t^{\eta\eta}$  and  $t^{\gamma\eta}$ , we did variations of  $A = t_n^{\gamma\eta}/t_p^{\gamma\eta}$ ,  $\text{Re } a_{\eta N}$  and  $\kappa$  within the corresponding uncertainty intervals. One of the most important parameters of the theory is the ratio of the photoproduction amplitudes for neutron and proton ( $A$ ). Six curves corresponding to different choices of  $A$  are depicted in Fig. 6. These curves were calculated with  $a_{\eta N} = (0.75, 0.30)$  fm and  $\kappa = \alpha = 3.316 \text{ fm}^{-1}$ . The experimental data are taken from Ref. [26].

In Fig. 7, we present the result of our calculations for five different choices of  $\text{Re } a_{\eta N}$ , namely, 0.55 fm, 0.65 fm, 0.725 fm, 0.75 fm, and 0.85 fm. This sequence of  $\text{Re } a_{\eta N}$  corresponds to the upward sequence of the curves in the near-threshold region. The parameters are:  $A = -0.75$  and  $\kappa = \alpha = 3.316 \text{ fm}^{-1}$ .

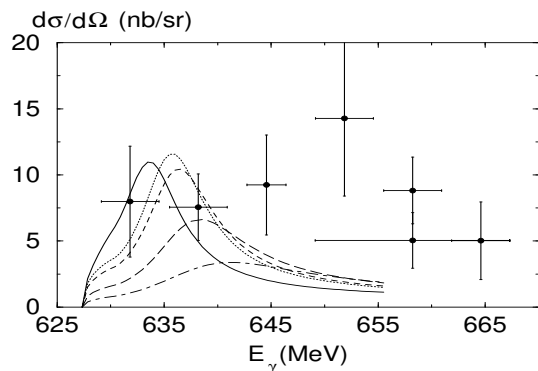


Figure 7: Differential cross-section ( $\Theta_\eta^{cm} = 90^\circ$ ) with different choices of  $\text{Re } a_{\eta N}$ .

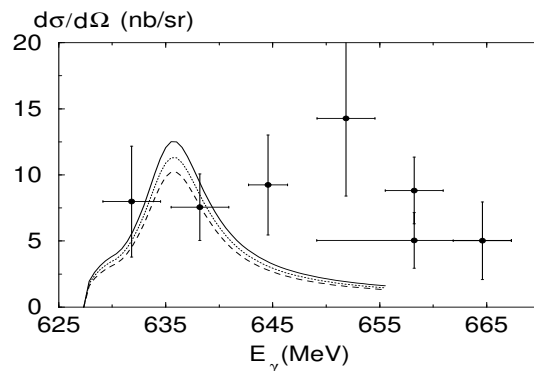


Figure 8: Differential cross-section with different choices of parameter  $\kappa$ .

In Fig. 8 the results of our calculations with three choices of the range parameter  $\kappa$  ( $2 \text{ fm}^{-1}$ ,  $3 \text{ fm}^{-1}$ , and  $5 \text{ fm}^{-1}$ ) of the electromagnetic vertex  $\gamma N \rightarrow S_{11}$  are given. These



curves correspond to  $a_{\eta N} = (0.75, 0.30)$  fm and  $A = -0.75$ . A comparison of the curves depicted in Figs. 6, 7 and 8 with the corresponding experimental data shows that no agreement with the data can be reached unless the ratio  $A$  is greater than  $-0.80$ .

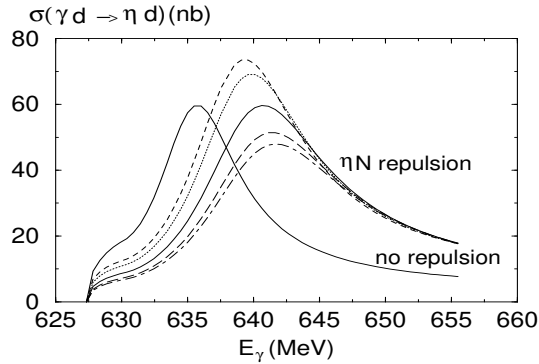


Figure 9: Shift of the resonant peak of the total cross-section due to the  $\eta N$  repulsion.

Under all variations of the parameters, however, the resonant peak remains about 15 MeV to the left of the experimental peak. Since this peak is due to the resonant final state interaction between the  $\eta$  meson and deuteron, we may expect that it can be shifted to the right by introducing a repulsion into the  $\eta N$  interaction. To introduce an  $\eta N$  repulsion which preserves the separable form of the corresponding T-matrix, we used the method suggested in Ref. [13] where a separable nucleon-nucleon T-matrix includes an energy dependent factor,  $b(E) = -\tanh(1 - E/E_c)$ . This factor causes the NN phase-shift to change sign at the energy  $E_c = 0.816$  fm $^{-1}$ , which is equivalent to presence of an NN repulsion. Since the purpose of our numerical experiment was to check if an  $\eta N$  repulsion could shift the peak to the right and there is no information about such repulsion, we used the same function  $b(E)$  and did variations of  $E_c$ , namely  $E_c/3$ ,  $E_c/2$ ,  $E_c$ ,  $2E_c$ , and  $3E_c$ . The corresponding curves are shown in Fig. 9 where the larger  $E_c$  the lower is the curve. All the curves depicted in Fig. 9 were calculated with  $a_{\eta N} = (0.75, 0.30)$  fm,  $A = -0.85$  and  $\kappa = \alpha = 3.316$  fm $^{-1}$ .

Therefore, comparison of our calculations with the experimental data suggests that  $A > -0.80$ ,  $\text{Re } a_{\eta N} > 0.75$  fm, and the  $\eta N$  interaction is likely to be repulsive at short distances. Our calculations are highly sensitive to the ratio of the photoproduction amplitudes for neutron and proton ( $A$ ) and depends rather weakly on the parameter  $\kappa$ .

Authors would like to thank Division for Scientific Affairs of NATO for support (grant CRG LG 970110) and DFG-RFBR for financial assistance (grant 436 RUS 113/425/1).

## References

- [1] A. Magiera, H. Machner, Nucl. Phys **A674** (2000) 515.
- [2] G. Hoehler,  $\pi N$  Newsletters **14** (1998) 168.

- [3] Q. Haider and L. C. Liu , Phys. Rev. Lett. **B172** (1986) 257.
- [4] M. Rößig-Landau *et al.*, Phys. Lett. **B373** (1996) 45.
- [5] C. Wilkin, Phys. Lett. **B331** (1994) 276.
- [6] H. C. Chiang, E. Oset, L. C. Liu, Phys. Rev. **C44** (1991) 738.
- [7] G. L. Li, W. K. Cheng, T. T. S. Kuo, Phys. Lett. **B195** (1987) 515.
- [8] A. M. Green, J. A. Niskanen, S. Wycech, Phys. Rev. **C54** (1996) 1970.
- [9] T. Ueda, Phys. Rev. Lett. **66** (1991) 297.
- [10] S. A. Rakityansky, S. A. Sofianos, M. Braun, V. B. Belyaev, and W. Sandhas, Phys. Rev. **C53** (1996) R2043.
- [11] N. V. Shevchenko, S. A. Rakityansky, S. A. Sofianos, V. B. Belyaev, and W. Sandhas, Phys. Rev. **C58** (1998) R3055.
- [12] F. Ritz and H. Arenhövel, Phys. Lett. **B447** (1999) 15.
- [13] H. Garcilazo, Lett. Nuovo Cim. **28** (1980) 73.
- [14] C. Bennhold and H. Tanabe, Nucl. Phys. **A530** (1991) 625.
- [15] Particle Data Group, Phys. Rev. **D50** (1994) 1173.
- [16] M. Batinic, I. Slaus, A. Svarc, Phys. Rev. **C52**, (1995) 2188.
- [17] A. M. Green, S. Wycech, Phys.Rev. **C55** (1997) R2167.
- [18] V. Yu. Grishina, L. A. Kondratyuk, M. Buescher, C. Hanhart, J. Haidenbauer, J. Speth, Phys. Lett. **B475** (2000) 9.
- [19] V. B. Belyaev, *Lectures in Few-Body Systems*, Springer Verlag.
- [20] F. Sohre and H. Ziegelman, Phys. Lett. **B34** (1971) 579.
- [21] N. Hoshy, H. Hyuga and K. Kubodera, Nucl. Phys. **A324** (1979) 234.
- [22] D. Halderson and A. S. Rosenthal, Nucl. Phys. **A501** (1989) 856.
- [23] Y. Zhang and D. Halderson, Phys. Rev. **C45** (1992) 563.
- [24] E. Breitmoser, H. Arenhoevel, Nucl. Phys. **A612** (1997) 321.
- [25] L. Tiator, C. Bennhold, S. S. Kamalov, Nucl. Phys. **A580** (1994) 455.
- [26] P. Hoffman-Rothe et al., Phys. Rev. Lett. **78** (1997) 4697.
- [27] A. Fix, H. Arenhoevel, Phys. Lett. **B492** (2000) 32.

- [28] B. Krusche et al., Phys. Rev. Lett. **74** (1995) 3736.
- [29] A. M. Green and S. Wycech, Phys. Rev. **C60** (1999) 035208.
- [30] N. C. Mukhopadhyay, J. F. Zhang, M. Benmerouche, Phys. Lett. **B364** (1995) 1.